Nanosecond-Regime Correlation Time Scales for Equilibrium Protein Structural Fluctuations of Metal-Free Cytochrome *c* from Picosecond Time-Resolved Fluorescence Spectroscopy and the Dynamic Stokes Shift

Jagnyaseni Tripathy[†] **and Warren F. Beck***

Department of Chemistry, Michigan State University, East Lansing, Michigan 48824, United States

Received: May 17, 2010; Revised Manuscript Received: September 30, 2010

We used picosecond time-resolved fluorescence spectroscopy to characterize the fluorescence Stokes shift (FSS) response function of metal-free (or free-base, fbCytc) cytochrome *c* under the solution conditions that favor the native states of ferricytochrome *c* (FeCytc) and Zn^{II}-substituted cytochrome *c* (ZnCytc). The intrinsic porphyrin chromophore serves in these experiments as a fluorescent probe of the structural fluctuations of the surrounding protein and solvent. Demetalation of the porphyrin destabilizes the folded structure of cytochrome *c* owing to the loss of the axial metal-histidine and metal-methionine bonds. Thus, these experiments examine how the time scales detected in a dynamic solvation experiment in a chromoprotein report changes in the character of motion. The FSS response function in fbCytc in water and pH 7 is well described by a biexponential response over the 100 ps to 50 ns regime with time constants of 1.4 and 9.1 ns; under similar conditions, ZnCytc exhibits a biexponential FSS response with time constants of 250 ps and 1.5 ns [Lampa-Pastirk and Beck, *J. Phys. Chem. B* **2004**, *108*, 16288]. These time constants correspond, respectively, to the correlation time scales for motions of the hydrophobic core and the solvent-contact layer of the protein. Both of the time constants observed in fbCytc are further lengthened upon addition of glycerol to the external solvent so that a significant fraction of the protein dynamics is rendered effectively static on the fluorescence time scale. The solvation reorganization energy, the time-integrated Stokes shift of the fluorescence spectrum, is reduced by about a third to 33 cm^{-1} in 50% glycerol from 43 cm^{-1} in water. These results are interpreted structurally using a model for Brownian diffusive motion with thermally activated barrier crossings on the protein-folding energy landscape. The results suggest that the mean-squared deviations of the structural fluctuations exhibited by fbCytc are nearly a factor of 10 larger than those of ZnCytc. This conclusion is consistent with the suggestion that fbCytc assumes a dynamic, partially unfolded structure with some of the characteristics of a molten globule.

1. Introduction

The energy landscape paradigm accounts for the molecular dynamics of folded proteins in terms of a hierarchy of conformational states sorted by tiers of intervening activation-energy barriers of increasing magnitude.[1−3] On the single-molecule level, a protein makes a diffusive search of the potential energy surface near the native structure by hopping from minimum to minimum over the barriers that are thermally accessible.[4,5] These motions correspond to what Frauenfelder calls equilibrium fluctuations.[2] Similar dynamics are expected to accompany the folding of a protein as it descends the funnel-shaped Gibbs free-energy gradient and approaches the native structure,[6] but the details of the motions that a protein makes as it searches for the native structure or when the structure is displaced from that at equilibrium by a perturbation deserve additional experimental and theoretical attention.

In recent work from this laboratory, we showed how Zn^{II}-substituted cytochrome *c* (ZnCytc) can be driven from the native fold to a series of partially unfolded structures by the intramolecular vibrational excitation generated by the vibrational relaxation of the intrinsic Zn^{II}-porphyrin chromophore.[7,8] When the 0−0 vibronic transition in the *Q* absorption band is pumped, so that the S_1 electronic state is prepared with very little excess vibrational energy, the time-resolved fluorescence spectrum exhibits a conventional, unidirectional dynamic fluorescence Stokes shift (FSS) response[9,10] to the red with two characteristic time scales, 250 ps and 1.45 ns. This response is assigned in analogy to that in polar liquids to a polar solvation response of the surrounding protein to the ground-to-excited-state change in the Zn^{II}-porphyrin's dipole moment. The two time scales were assigned to motions of the hydrophobic core and solvent-contact layers of the protein, respectively, because addition of glycerol to the external solvent medium slowed only the latter component. When the excitation wavelength was set at 420 nm in the Soret band, so that that the S_1 state is prepared with ∼7000-cm^{-1} excess vibrational energy, the Zn^{II}-porphyrin in ZnCytc exhibits an unusual bidirectional FSS response that directly reports a change in the surrounding protein structure. The time-resolved fluorescence spectrum shifts initially to the red with a 125-ps time constant; after the 180-ps delay point, however, the spectrum begins a slower, biexponential shift to the blue that persists to the end of the fluorescence time scale (>12 ns). The blue-shifted fluorescence spectrum is assigned to a partially unfolded state of the protein that transiently resembles that of the molten-globule state observed under acid conditions;[11,12] the heat-denatured state of ZnCytc also exhibits a blue-shifted fluorescence spectrum.[13]

Subsequent work[8] showed that as the excitation wavenumber is tuned to the blue, the continuous-wave fluorescence spectrum

* Corresponding author. E-mail: beckw@msu.edu. Fax: 517-353-1793.
[†] Graduate student, Department of Physics.

10.1021/jp1044964
Published on Web 11/15/2010

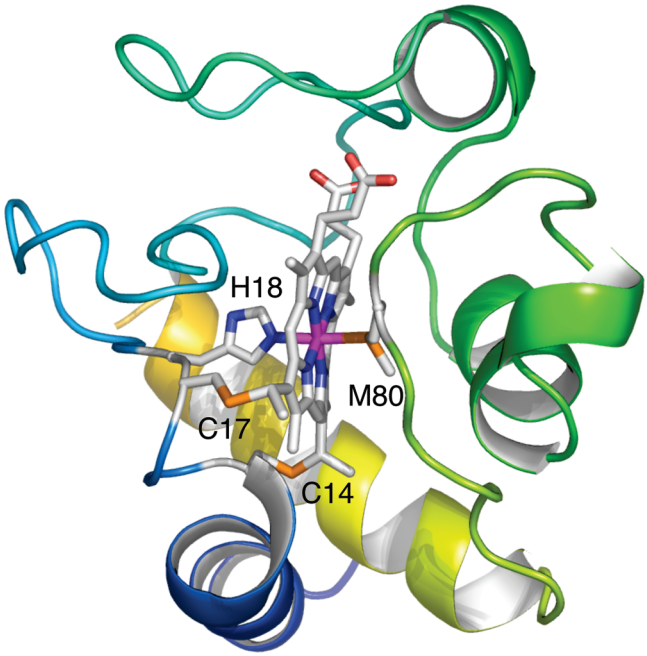

Figure 1. Structure of ferricytochrome *c* from horse heart (1hrc.pdb).[15] The porphyrin, its thioether linkages from cysteine ligands C14 and C17, and the axial ligands to the metal ion, from the histidine and methionine residues H18 and M80, respectively, are rendered as stick structures.

from ZnCytc reports the activation-enthalpy thresholds to at least three partially unfolded states in terms of step-like transitions of the solvation reorganization energy,[14] the time-integrated Stokes shift of the fluorescence spectrum. The corresponding barriers in metal-free (or free-base, fbCytc) cytochrome *c* occur at relatively low activation enthalpies, perhaps one-third of those in ZnCytc. This finding shows that the axial metal−histidine (H18) and metal−methionine (M80) bonds in cytochrome *c* play an important structural role (see Figure 1). Under the solution conditions that favor the native state of ferricytochrome *c* (FeCytc) or ZnCytc, it is likely that fbCytc exists as a partially unfolded, molten-globule-like structure that retains a well-defined hydrophobic core like that of ZnCytc.[8]

In this contribution, we report the FSS response obtained from fbCytc with the excitation laser tuned close to the 0−0 vibronic transition. This work allows a comparison to the previously reported FSS response observed in the native state of ZnCytc.[16] These experiments provide a unique opportunity to determine how the time scales detected in a dynamic solvation experiment in a chromoprotein report changes arising from a structural perturbation. The results show that the two exponential time constants observed in the FSS response from fbCytc are lengthened by almost a factor of 10 from those of ZnCytc and that both components are sensitive to the presence of glycerol in the external solvent medium. By applying a model for the structural fluctuations that arise from Brownian diffusion on the protein-folding energy landscape,[17] we infer that the increased polar solvation time scales observed in fbCytc correspond to significantly enhanced fluctuation amplitudes compared to those in ZnCytc under similar solvent conditions.

2. Experimental Section

Sample Preparation. The procedure established by Vanderkooi and co-workers[18,19] was used to prepare fbCytc using horse-heart FeCytc (Sigma) as the starting material. The free-base porphyrin is obtained in situ using liquid anhydrous hydrogen fluoride (HF) as the demetalating agent. The reaction of FeCytc with HF was run on a home-built gas-handling system that employs tubing, valves, and reaction vessels all made of Teflon. The extent of the demetalation reaction was monitored spectrophotometrically using the vibronic structure of the *Q*-band region of the absorption spectrum. The fbCytc product was worked up using methods adapted from those employed by Winkler and co-workers[20] and Kostić and co-workers.[21] After desalting, the protein was isolated by cation-exchange chromatography first on a Whatman CM-52 column and optionally then on a Mono-S 4.6/100 PE FPLC column (GE Healthcare Life Sciences). Fractions corresponding to fbCytc were combined and then were equilibrated with a 25 mM sodium phosphate buffer solution at pH 7.0 by repeated concentration using an Millipore YM10 ultrafilter and dilution with the buffer solution. After a final ultrafiltration step, the product was analyzed on a Superdex 75 FPLC gel-filtration column (GE Healthcare Life Sciences). This procedure yields fbCytc free of the low molecular-weight polypeptide contaminants that are typically observed directly from the HF demetalation reaction. The concentrated fbCytc solution obtained from the final ultrafiltration step was divided into small aliquots and then flash-frozen in liquid nitrogen. The frozen samples were stored in a −85 °C freezer for up to a year.

For use in fluorescence spectroscopy, one of the frozen samples was thawed and then diluted with 25 mM phosphate buffer solution at pH 7.0 or with a glycerol-buffer solution mixture (50% glycerol by volume). The final protein solution was then passed through a 0.22 μM microfilter to remove any large debris. The sample's concentration was then adjusted by adding additional diluent solution so that the absorption at the peak of the Q_y absorption band for a path length of 1.0 cm ranged from 0.1−0.2. The sample was held in quartz cuvettes with the headspace purged with dry nitrogen gas prior to an experiment.

Continuous-Wave Absorption and Fluorescence Spectroscopy. Absorption spectra were acquired with a Hitachi U-2000 spectrophotometer (2-nm bandpass). Fluorescence spectra were obtained with a home-built spectrofluorimeter[8] consisting of an Jobin-Yvon AH10 100-W tungsten-halogen light source, a Jobin-Yvon H10 excitation monochromator (4-nm bandpass), an Acton Research SP-150 emission spectrograph (2-nm bandpass), and a Jobin-Yvon Symphony charge-coupled device (CCD) detector. The CCD detector employs a liquid nitrogen cooled, back-illuminated, 2000 × 800 pixel silicon detector chip (EEV corporation). The sample cuvette was held in a Quantum Northwest TLC50F Peltier-effect temperature controller. As presented as a function of wavenumber, the fluorescence intensities are multiplied by the square of the wavelength in order to compensate for the fixed (in wavelength units) spectral bandpass of the emission spectrograph.[22] The absorption and fluorescence instruments were controlled by LabVIEW (National Instruments) programs.

Picosecond Time-Resolved Fluorescence Spectroscopy. Single-wavelength fluorescence transients were acquired with a time-correlated, single photon counting (TCSPC) system operated in the reverse triggered mode. This instrument was described in detail in an earlier contribution.[23] Excitation pulses were obtained from a synchronously pumped, cavity-dumped rhodamine-6G dye laser (Coherent 702−1), which was pumped by the 532-nm second-harmonic output of a mode-locked Nd^{III}-YAG laser (Coherent Antares 76-S). The cavity dumper on the dye laser was operated at 4 MHz, so the excitation interpulse period was 250 ns. The zero-background autocorrelation width

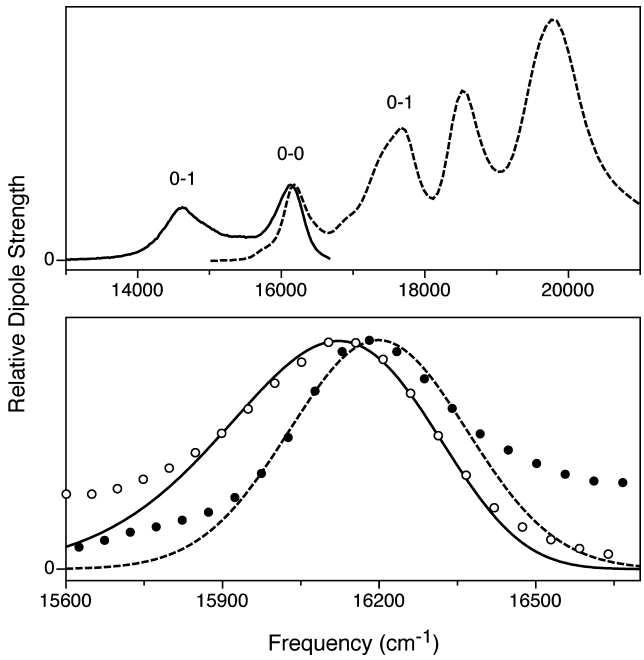

Figure 2. Top panel: Continuous-wave absorption (dashed) and fluorescence emission (solid) spectra from metal-free cytochrome *c* (fbCytc) in water at 22 °C and pH 7, plotted as relative dipole strengths, $A(\nu)/\nu$ and $F(\nu)/\nu^3$, respectively. The fluorescence spectrum was obtained with the excitation light source tuned to 16130 cm^{-1} (620 nm). Bottom panel: Detailed view of the 0−0 region, with the data points shown superimposed with log-normal line shapes (see Table 1 for the fit parameters).

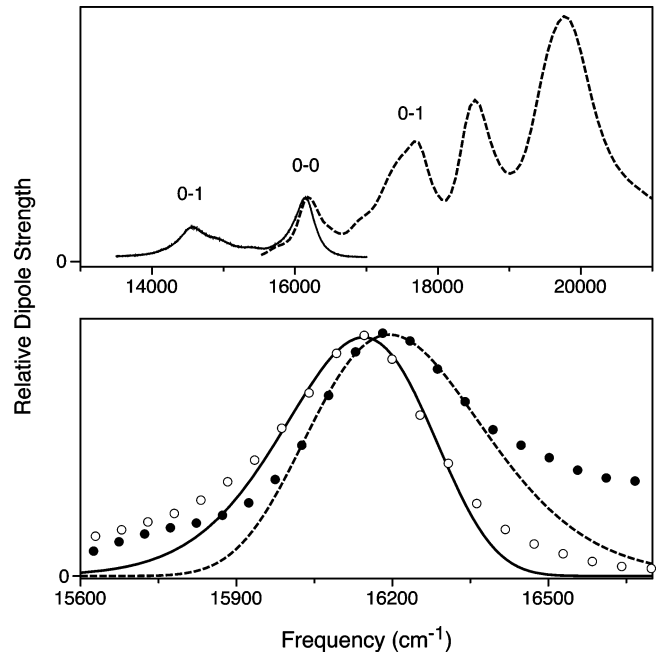

Figure 3. Top panel: Continuous-wave absorption (dashed) and fluorescence emission (solid) spectra from fbCytc in 50% (v/v) glycerol at 22 °C and pH 7, plotted as relative dipole strengths, $A(\nu)/\nu$ and $F(\nu)/\nu^3$, respectively. The fluorescence spectrum was obtained with the excitation light source tuned to 16130 cm^{-1} (620 nm). Bottom panel: Detailed view of the 0−0 region, with the data points shown superimposed with log-normal line shapes (see Table 1 for the fit parameters).

of the excitation pulses was 5 ps, as measured using an Inrad 5−14A autocorrelator. The fluorescence emission was collected at 90° from the excitation laser beam and was analyzed by a calcite polarizer set to the magic angle with respect to the plane of the excitation laser so that dichroism-free transients were acquired. The emission was then detected using a double subtractive monochromator (CVI CM112) and a microchannel-plate photomultiplier tube (Hamamatsu R3809U-51), the output of which was analyzed using a NIM-based TCSPC setup as previously described. The instrument-response function obtained with a dilute scattering solution at the sample position had a width (fwhm) of approximately 100 ps in these experiments. A LabVIEW (National Instruments) program controlled the emission monochromator and the photon-counting hardware so that a set of single-wavelength fluorescence transients over a range of emission wavelengths across the fluorescence spectrum could be automatically acquired. The sample was held in a water-cooled mount, which was maintained at 22 °C with a Neslab 221 water circulator.

3. Results

Continuous-Wave Absorption and Fluorescence Emission Spectra. Figures 2 and 3 show the absorption ($A(\nu)$) and fluorescence ($F(\nu)$) spectra obtained at 22 °C from fbCytc at pH 7.0 in water and 50% (v/v) glycerol, respectively. The spectra are plotted with respect to wavenumber ν as relative dipole strengths, $A_D(\nu) = A(\nu)/\nu$ and $F_D(\nu) = F(\nu)/\nu^3$, respectively.[22,24,25] The plotted region shows the *Q* band, which consists of a pair of partially resolved vibronic bands from the *x* and *y* polarized transition-dipole moments in the plane of the Zn^{II} porphyrin. The fluorescence spectrum's 0−0 and 0−1 peaks exhibit an approximate mirror-symmetry with respect to the two lowest wavenumber features, the 0−0 and 0−1 peaks from the Q_y transition. The relative scaling of the absorption and fluorescence spectra in Figures 2 and 3 was set so that the 0−0 peaks have the same intensities.

TABLE 1: Lognormal and Gaussian Lineshape Models for the 0−0 Peak in the Absorption (A) and Fluorescence (F) Spectra from fbCytc in Water and in 50% (*v*/*v*) Glycerol (see Figures 2 and 3) and Estimates for the Solvation Reorganization Energy (λ)

	water		50% (*v*/*v*) glycerol	
parameter[a]	Lognormal	Gaussian	Lognormal	Gaussian
$\nu_{0-0,A}$	16198 cm^{-1}	16199 cm^{-1}	16194 cm^{-1}	16201 cm^{-1}
$\Delta\nu_{0-0,A}$	426 cm^{-1}	408 cm^{-1}	396 cm^{-1}	370 cm^{-1}
$\rho_{0-0,A}$	1.13		1.22	
$\nu_{0-0,F}$	16122 cm^{-1}	16133 cm^{-1}	16144 cm^{-1}	16135 cm^{-1}
$\Delta\nu_{0-0,F}$	476 cm^{-1}	465 cm^{-1}	396 cm^{-1}	337 cm^{-1}
$\rho_{0-0,F}$	1.22		1.22	
λ	38 cm^{-1}	43 cm^{-1}	25 cm^{-1}	33 cm^{-1}

[a] See eq 1 and the text.

In order to determine the changes in spectral line shape and position that are induced by the change of solvent from water to 50% glycerol, we fit the 0−0 peaks of the absorption and fluorescence dipole-strength spectra to Gaussian and log-normal[26] lineshapes. The lower panels of Figures 2 and 3 show the log-normal lineshapes superimposed on an expanded view of the 0−0 peaks. The fit parameters listed in Table 1 include the center frequencies (ν_{0-0}), the widths (fwhm, $\Delta\nu_{0-0}$) and for the log-normal lineshapes, the asymmetry (or skew) parameter (ρ_{0-0}). Estimates for the solvation reorganization energy, λ, were then obtained as one-half the difference between the center frequencies of the absorption (A) and fluorescence (F) 0−0 peaks

$$\lambda = (\nu_{0-0,A} - \nu_{0-0,F})/2 \quad (1)$$

Using the ν_{0-0} parameters from the fitted log-normal lineshapes, this equation returns values for λ of 38 cm^{-1} in water and 25 cm^{-1} in 50% glycerol. These estimates are valid if the ground-state and excited-state potential-energy surfaces are harmonic and have the same normal-mode frequencies,[27,28] which is the case if the absorption and fluorescence spectra exhibit an exact mirror symmetry with respect to frequency. An additional formal requirement for the applicability of eq 1 is that the vibronic lineshapes are Gaussians.[29] The estimates for λ are somewhat larger in both solvents if Gaussian lineshapes are used to fit the 0−0 peaks (43 and 33 cm^{-1}, respectively). Still, these peak-shift estimates for λ should be regarded as lower limits. Because the 0−0 peaks are only partially resolved, it is not possible to apply rigorously the equation for λ introduced by Fleming and co-workers[29]

$$\lambda = \frac{\int_0^\infty d\nu\, \nu[\sigma_a(\nu) - \sigma_f(\nu)]}{\int_0^\infty d\nu\, [\sigma_a(\nu) + \sigma_f(\nu)]} \quad (2)$$

which integrates over the absorption (σ_a) and fluorescence (σ_f) spectra and avoids assumptions about the lineshapes. When applied to the spectra shown in Figures 2 and 3, eq 2 obtains estimates for λ that are about a factor of 2 larger than those listed in Table 1. This scaling of estimates for λ using eqs 1 and 2 is similar to that obtained by Fleming and co-workers for eosin in water and for lysozyme labeled with eosin.[29]

The reduction by at least a third of the solvation reorganization energy for fbCytc that accompanies the change from water to 50% glycerol (see Table 1) is too large to be explained only by the change in solvent. Using a dielectric continuum treatment of the solvent surrounding a probe chromophore, the Lippert−Mataga equation[22,30,31] relates the solvation reorganization energy to the dielectric constant, ε_0, and the index of refraction, n, in a given solvent mixture

$$\lambda = \frac{\Delta\mu_{eg}^2}{hca^3}\left[\frac{\varepsilon_0 - 1}{2\varepsilon_0 + 1} - \frac{n^2 - 1}{2n^2 + 1}\right] \quad (3)$$

The first term in this equation depends on the probe; it indicates that λ depends on the ground-to-excited-state change in the probe's dipole moment, μ_{eg}, and the radius of the surrounding spherical solvent cavity, a. If these parameters are held constant, λ is reduced only by about ten percent by changing the parameters in the bracketed expression from those for water ($\varepsilon_0 = 80.37$, $n = 1.3326$) to those for 50% (v/v) (or 56% (w/w)) glycerol/water ($\varepsilon_0 = 64$, $n = 1.4063$) at 25 °C.[32,33] This estimate would be appropriate if the porphyrin chromophore in fbCytc is fully solvated by the external solvent, but it is probable that the porphyrin is almost fully solvated by the surrounding protein structure; Table 1 shows that the fluorescence spectrum is only shifted a few cm^{-1} to the blue by the change from water to 50% glycerol. In contrast, the fluorescence spectrum from ZnCytc shifts 50 cm^{-1} to the blue when water is replaced by 50% glycerol. Such a shift is consistent with the partial exposure to the external solvent of the edge of the porphyrin macrocycle that is indicated by the FeCytc crystal structure (see Figure 1). The change in solvent to 50% glycerol has little or no effect, however, on λ for ZnCytc; the same value, $\lambda = 145$ cm^{-1}, is observed in water and in 50% glycerol.[16]

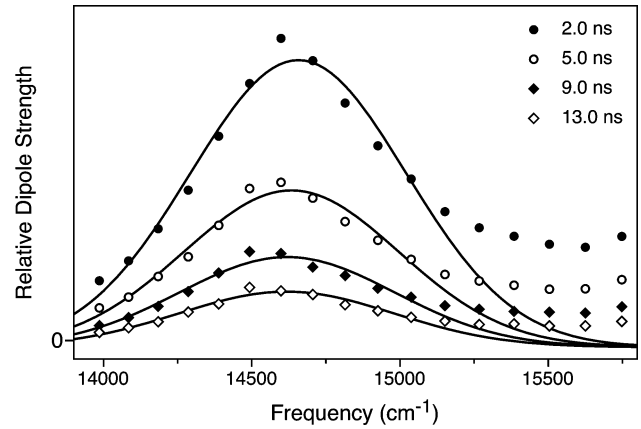

Figure 4. Time-resolved fluorescence dipole strength spectra from fbcytc in water at 22 °C at four time delays. The displayed spectral region corresponds to the 0−1 peak. The spectra are superimposed with fitted log-normal line shapes.

Picosecond Time-Resolved Fluorescence Spectroscopy. Since the dielectric properties of the external solvent account only for a small fraction of the reduction of the solvation reorganization energy, λ, that accompanies changing the solvent from water to 50% glycerol, it is likely that the average time scale for the solvation response of the protein in fbCytc is lengthened enough in the presence of 50% glycerol so that some of the motions are slowed enough that they do not contribute to λ. These conclusions are supported by the measurements of the FSS response function that are described next.

Time-resolved fluorescence spectra from fbCytc in water and in 50% glycerol were obtained as slices from a time-wavelength-intensity (dipole-strength) surface $F_D(\nu, t)$ that spanned the 0−50 ns by 13 500−16 000 cm^{-1} region. The excitation laser was fixed at 16 130 cm^{-1}, which is near to the wavenumber of the 0−0 transition in water and 50% glycerol, respectively (see Figures 2 and 3). The surface was acquired as a set of single-wavelength transients spaced by 5.0 nm (∼130 cm^{-1} at 620 nm), the bandpass of the emission monochromator. The emission tuning range spans the 0−1 peak and continues nearly to the maximum of the 0−0 peak. Owing to the 5-nm bandpass of the emission monochromator and the relatively small value for λ, we were unable to work further to the red than the maximum of the 0−0 peak because of interference from scattering from the excitation laser. Because the transients were recorded over the 0−50-ns delay range, a span of 25 times the fluorescence lifetime under the chosen sample conditions, the time-wavelength-intensity surface was constructed by normalizing the integral of each transient to the fluorescence dipole strength observed in the continuous-wave spectrum at the emission wavenumber of the transient. The transients were then used directly, without deconvolution of the instrument-response function, and they were truncated so that the first data point employed in further analysis was that of the 100-ps delay, a full instrument-response width after the center of the excitation pulse.

Figure 4 shows a set of time-resolved fluorescence dipole-strength spectra from fbCytc in water at 22 °C. The spectra were obtained as slices from the $F_D(\nu, t)$ time-wavelength-intensity surface at four delay times t. Fitted log-normal lineshapes are shown superimposed on the data points. As the time delay increases, the spectra decay in intensity and the wavenumber of the peak maximum shifts to lower frequency. The time evolution of the mean fluorescence dipole strength

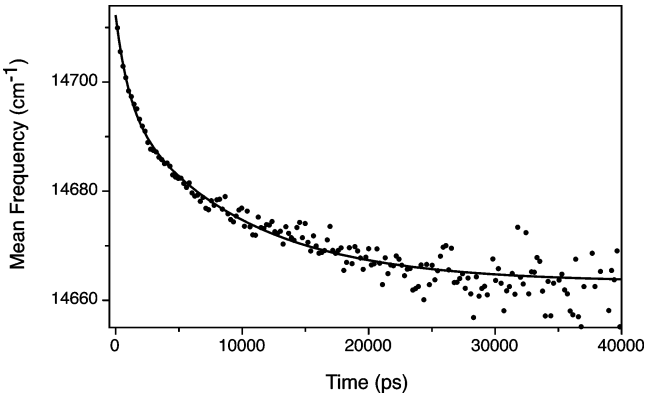

Figure 5. Time evolution of the mean emission frequency of the 0−1 fluorescence transition, $\langle \nu_{0-1} \rangle$, from fbCytc in water at 22 °C. The data points are superimposed on a fitted double-exponential model. The fit parameters are listed in Table 2.

for the 0−1 peak, $\langle \nu(t) \rangle$, was obtained by integrating over the time-resolved spectrum at a given time t

$$\langle \nu(t) \rangle = \frac{\int_{\nu_1}^{\nu_2} \mathrm{d}\nu \; \nu F_{\mathrm{D}}(\nu, t)}{\int_{\nu_1}^{\nu_2} \mathrm{d}\nu \; F_{\mathrm{D}}(\nu, t)} \tag{4}$$

The $\langle \nu(t) \rangle$ response is used in the following without normalization as a direct measure of the FSS response function (eq 5) over the 100 ps to 50 ns regime. This practice avoids the need to estimate the mean fluorescence emission frequencies at zero time and at infinite time (see also the discussion on this issue in ref 34). The response shown in Figure 5 is well described by a biexponential decay function. The limits for the integral, $\nu_1 = 14\,000$ cm^{-1} and $\nu_2 = 15\,500$ cm^{-1}, were selected so that the range of integration spanned the 0−1 peak but avoided the onset of the 0−0 peak. The calculated $\langle \nu(t) \rangle$ response is essentially invariant with different choices of ν_1 and ν_2, but the fitted $t = \infty$ asymptote varies over a few wavenumbers depending on how far the integration extends over the congested region between the 0−1 and 0−0 peaks. In the previous work on ZnCytc,[16] $\langle \nu(t) \rangle$ was determined from the time evolution of the fluorescence 0−0 transition frequency, which was obtained from a fitted vibronic progression for the 0−0 and 0−1 peaks. The use of the mean-frequency calculation in the present work allows us to obtain a robust measurement of the FSS response function despite the smaller solvation reorganization energy and the poorer signal/noise ratio of the fbCytc data sets. A similar approach was used previously by Toptygin et al. in their study of dynamic solvation in single-tryptophan mutants of IIA$^{\mathrm{Glc}}$ protein.[35]

The addition of glycerol to the fbCytc solution results in a significant slowing of the FSS response function. Two exponential components are observed, just as in water, but the total shift to the red is smaller than observed in water (see Figures 6 and 7). The time constants observed in 50% glycerol, 3.18 and 13.71 ns, are lengthened significantly compared to those observed in water, 1.37 and 9.06 ns, respectively (see Table 2). The reduction of λ indicated by the continuous-wave spectra (Figure 3) and by the $\langle \nu(t) \rangle$ response (Figure 7) further requires that a portion of the motion observed in water is rendered effectively static relative to the fluorescence time scale in 50% glycerol.

Table 2 also lists the parameters that describe the FSS response function observed previously from ZnCytc under similar conditions.[16] Both of the time constants observed in ZnCytc are almost ten times shorter than those of fbCytc. Note that only the slower of the two components observed from ZnCytc is affected significantly by the addition of glycerol to the external solvent medium (see Table 2). That the solvation reorganization energy for ZnCytc in water is the same as that in 50% glycerol[16] supports the conclusion that the addition of glycerol primarily acts on the FSS response by damping the motions of groups in the solvent-contact layer of the protein; the studies by Vincent et al.[36] suggest that this frictional action of glycerol involves changes of the structure and dynamics of water molecules in the hydration layer. The results observed

TABLE 2: Model Parameters for the Time Evolution of the Time-Resolved Fluorescence Spectrum Observed in Water and 50% Glycerol in Metal-Free (fbCytc) and Zn$^{\mathrm{II}}$-Substituted (ZnCytc) Cytochrome *c* at 22 °C

Protein	Solvent	A_1, cm^{-1}	τ_1, ns	A_2, cm^{-1}	τ_2, ns	ν_∞, cm^{-1}
fbCytc[a]	water	13.9	1.37	36.5	9.06	14663
	50% glycerol	18.4	3.18	11.4	13.7	14621
ZnCytc[b]	water	70	0.250	100	1.450	16940
	50[b]	60	0.260	90	2.200	17000

[a] $\langle \nu_{0-1}(t) \rangle = A_1 \mathrm{e}^{-t/\tau_1} + A_2 \mathrm{e}^{-t/\tau_2} + \nu_\infty$, see eq 4 and the text. [b] From ref 16; $\langle \nu_{0-0}(t) \rangle = A_1 \mathrm{e}^{-t/\tau_1} + A_2 \mathrm{e}^{-t/\tau_2} + \nu_\infty$, from a fitted vibronic progression over the 0−0 and 0−1 region of the fluorescence spectrum.

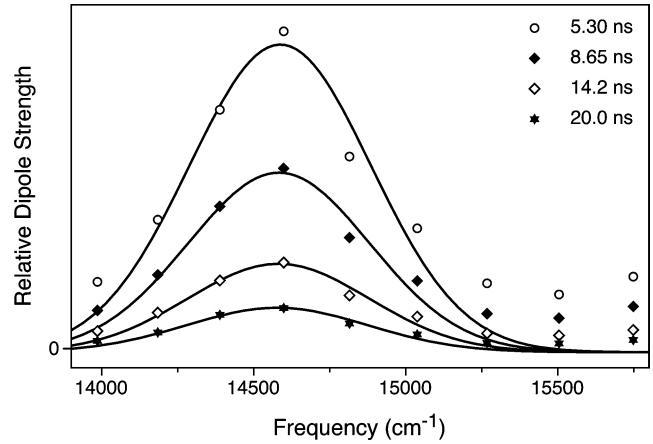

Figure 6. Time-resolved fluorescence dipole strength spectra from fbcytc in 50% (v/v) glycerol at 22 °C at four time delays. The displayed spectral region corresponds to the 0−1 peak. The spectra are superimposed with fitted log-normal line shapes.

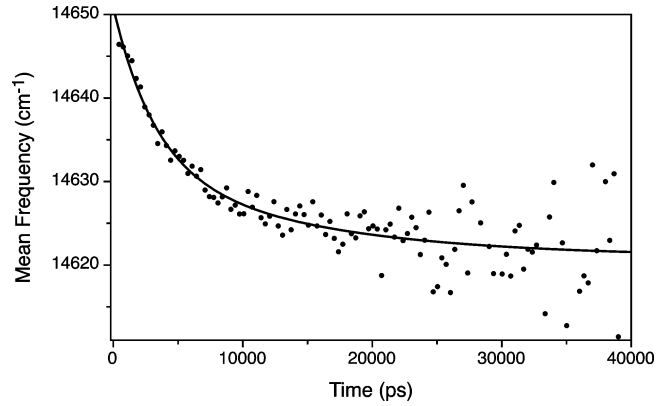

Figure 7. Time evolution of the mean emission frequency of the 0−1 fluorescence transition, $\langle \nu_{0-1} \rangle$, from fbCytc in 50% (*v*/*v*) glycerol at 22 °C. The data points are superimposed on a fitted double-exponential model. The fit parameters are listed in Table 2.

here with fbCytc evidence a similar structural order of assignment for the two time scales in the FSS response but with an even larger effect of the solvent friction than observed with ZnCytc.

4. Discussion

The main finding of this paper is that the FSS response function measured for fbCytc over the 100 ps to 50 ns time scale is significantly slower than that of ZnCytc under the solution conditions that favor the native folded state. The motions that are sensed by the intrinsic porphyrin chromophore in this time scale regime are predominantly from fluctuations of the surrounding protein structure. In the following, we review the current thinking about the origin of the FSS response in chromoproteins that supports this assignment, and then we consider how the correlation time scales observed in the FSS response function of fbCytc and ZnCytc can be interpreted structurally in terms of Brownian diffusive motion on the protein-folding energy landscape. The effect of external solvent friction is included by incorporating an Arrhenius expression relating the barrier heights that divide the minima on the energy landscape to the correlation time scales for the fluctuations. Overall, the analysis supports the conclusion that the slowing of the FSS response function in fbCytc arises from an increase in the mean-square displacements of the core and surface fluctuations compared to those in ZnCytc. These conclusions are consistent with the suggestion that the equilibrium structure of fbCytc is a partially unfolded, molten-globule-like state.

Solvent-Response Functions in Liquids and Proteins. The FSS or solvent-response function, $S_\nu(t)$,[9,10,14,37] describes the reorganizational response triggered in a condensed phase medium by the ground-to-excited-state change in the probe's dipole moment that accompanies its optically driven absorption transition. It is usually defined in terms of the time evolution of the mean frequency of the time-resolved fluorescence spectrum, $\langle\nu(t)\rangle$, as

$$S_\nu(t) = \frac{\langle\nu(t)\rangle - \langle\nu(\infty)\rangle}{\langle\nu(0)\rangle - \langle\nu(\infty)\rangle} \tag{5}$$

In polar liquids, most of the properties of $S_\nu(t)$ observed experimentally can be calculated by treating the liquid medium as a dielectric continuum.[9,31] Here the optical transition of the probe is treated as applying a step-function change in the electric field that is sensed by the surrounding solvent molecules. In the simplest picture, given the parameters from a description of the liquid's frequency dependent dielectric response, $\varepsilon(\omega)$, using a single Debye dispersion,

$$\varepsilon(\omega) = \varepsilon_\infty + \frac{\varepsilon_0 - \varepsilon_\infty}{1 - i\omega\tau_D} \tag{6}$$

the calculated solvation response is a single exponential function with a time constant

$$\tau_F = \left(\frac{2\varepsilon_\infty + \varepsilon_c}{2\varepsilon_0 + \varepsilon_c}\right)\tau_D \tag{7}$$

In these equations, ε_∞ and ε_0 are the infinite-frequency and zero-frequency (static) dielectric constants and τ_D is the dielectric (Debye) relaxation time. The parameter ε_c is the dielectric constant of the cavity in the solvent medium that surrounds the probe chromophore; it can be calculated knowing the structure of the probe and the polarizability of the solvent medium. Because usually $\varepsilon_0 \gg \varepsilon_\infty$ and $\varepsilon_0 \gg \varepsilon_c$, the solvation time constant τ_F is equal to the longitudinal relaxation time constant[9,31,38]

$$\tau_L = (\varepsilon_\infty/\varepsilon_0)\tau_D \tag{8}$$

This result indicates that $\tau_F \ll \tau_D$.[38] In polar solvents, τ_F is predominantly determined by the time scale for rotational diffusion. At very short time scales, hindered rotations (librations)[38] and inertial (free-rotor) motions[39−44] make major contributions to the solvent-response function.

The molecular character of $S_\nu(t)$ is usually discussed in terms of the fluctuations of the local electric field that arise from the random motions of the solvent dipoles around the probe chromophore. In the time domain, the probe's ground-to-excited state transition frequency $\omega = 2\pi\nu$ exhibits fluctuations

$$\Delta\omega(t) = \langle\omega\rangle - \omega(t) \tag{9}$$

from that averaged over time or averaged instantaneously over the ensemble. The fluctuations are characterized by a time-correlation function

$$M(t) = \frac{\langle\Delta\omega(0)\Delta\omega(t)\rangle}{\langle(\Delta\omega)^2\rangle} \tag{10}$$

which describes the associated loss of memory over time of the instantaneous transition frequency $\omega(0)$ that was present initially at some reference time $t = 0$. At high temperatures and in the linear-response regime, where the fluctuation−dissipation relation holds, $M(t)$ is equal to the solvent-response function $S_\nu(t)$.[9,45,46] The requirement for the linear-response regime is generally met in most probe/solvent systems because the optical excitation of the probe results only in a small change in the probe's dipole moment and accordingly presents a small perturbation to the motions and structure of the solvent.[47,48] Note that the three-pulse stimulated photon-echo peak shift (3PEPS) response is usually taken as being a direct measure of $M(t)$.[45,46] In several systems, however, the 3PEPS response includes components from intramolecular nonradiative electronic state dynamics in addition to those arising from solvation dynamics.[37,49,50] Given knowledge of $M(t)$, or of the spectral density, $\rho(\omega)$, which is obtained as its Fourier transform, it is possible to calculate all of the spectroscopic observables for the probe/solvent system. For example, the solvation reorganization energy, λ, is equivalent to the mean frequency of the spectral density[14,46]

$$\lambda = \hbar\int_0^\infty d\omega\, \omega\rho(\omega) \tag{11}$$

The studies of dynamic solvation in small proteins using transient holeburning, time-resolved fluorescence, or stimulated photon-echo methods have targeted predominantly the <100-ps regime that is readily probed by femtosecond spectroscopy.[49,51−58] Even when sensed by electronic probes located in the interior of a protein, the motions of water molecules in the bulk or in the hydration layer surrounding proteins still make dominant contributions to the detected response function and especially at short times (<1 ps).[29,59] Because the effective dielectric constant in the interior of a protein

is small,[60] the electric-field fluctuations sensed by the probe from water molecules in the surroundings are poorly screened by the protein medium. In liquid water, $M(t)$ decays according to two phases, the inertial (<100 fs, Gaussian) and diffusive reorientational (<1 ps, exponential) responses.[41] In a number of studies, components in the FSS response with time constants as long as 100 ps have been assigned to motions of water molecules as they exchange between sites on the surface of proteins and the hydration layer.[53−55,61−63] In contrast, Nilsson and Halle[48] argued that the FSS response cannot sense these water motions because the exchange reactions would not be accompanied by a modulation of the local electric field; replacement of a bound water molecule with a free water molecule from the bulk would occur in a concerted fashion. Using the results from molecular dynamics (MD) simulations that featured calculations of the dielectric response of the protein and surrounding solvent at each step in the trajectory, they concluded instead that the motions of water molecules in the hydration layer are only somewhat slowed from those in the bulk solvent, with <1.5-ps correlation times being characteristic. Slower correlation times in the response function were assigned only to the motions of protein-derived groups as the time scales increase into the >10-ps range and longer.[48] These conclusions are strongly supported by the recent MD simulations of Toptygin et al., but these authors add the interesting observation that their calculated response functions poorly reproduce the experimentally observed FSS time scales when protein motions are predominantly involved.[34]

There have been only a few observations of protein-derived motions using dynamic solvation methods in the >100-ps regime of time featured in the present work because the probe has usually been located in a binding site that is adjacent to or on the solvent-contact surface, where the electric-field fluctuations are dominantly those from the external water molecules. The very first picosecond time-resolved fluorescence investigations of dynamic solvation in small proteins, in the McLendon[64] and Boxer[65] laboratories, accessed ps-ns motions in apomyoglobin using extrinsic solvatochromic probes in the heme-binding site. Vincent et al.[36] used the single tryptophan residue in cytidine monophosphate kinase from *Escherichia coli* as a fluorescent probe in studies of the FSS response of the protein over the 100-ps-ns regime. Toptygin et al. subsequently characterized the solvation response over the 100-ps-10-ns regime in single-tryptophan-containing mutants of the IIA^{Glc} protein[35] and in the B1 domain fragment (GB1) of *Streptococcus* protein G.[66]

We chose to characterize the FSS response of ZnCytc in our previous work[16,23] because the intrinsic porphyrin could be exploited as a fluorescent probe that senses both internal and surface motions of the protein owing to its central position in the structure and its span to the solvent-contact surface via a cleft that mediates its physiological role in electron transfer (see Figure 1). The present study of fbCytc extends the work on ZnCytc by showing that the time scales assigned to the hydrophobic core and surface-contact layers are both lengthened in fbCytc and that no new time scales are detected. In contrast to the work on GB1 noted above,[66] the FSS response functions in both ZnCytc and fbCytc are well described by the sum of exponential components. This finding suggests that what is observed in fbCytc and ZnCytc are well isolated characteristic time scales for discrete protein motions. This point is significant especially because fbCytc is a partially unfolded structure under the equilibrium solution conditions used in the present experiments.

Activated Barrier-Crossing Model for Protein Fluctuations. While it would be obviously desirable eventually to compare the present FSS results with a full MD simulation of the time evolution of the dielectric response, as has been done for the protein G system mentioned above,[34,56,66−68] the long time scales we observed experimentally for fbCytc would necessitate the calculation of especially long MD trajectories to obtain convergence of the calculated time-correlation functions for the structural fluctuations. An additional critical problem is that the fbCytc system does not have a well-defined starting structure. In order to discuss further the structural implications of the lengthened FSS time scales detected in fbCytc, we apply in the following a model for the fluctuation time scales that would arise from diffusive motion on the protein-folding energy landscape. The goal of this analysis is to provide a reasonable framework for an interpretation of both the change in time scale that arises upon demetalation of ZnCytc to obtain fbCytc and also the effect of the change in solvent friction that occurs upon addition of glycerol.

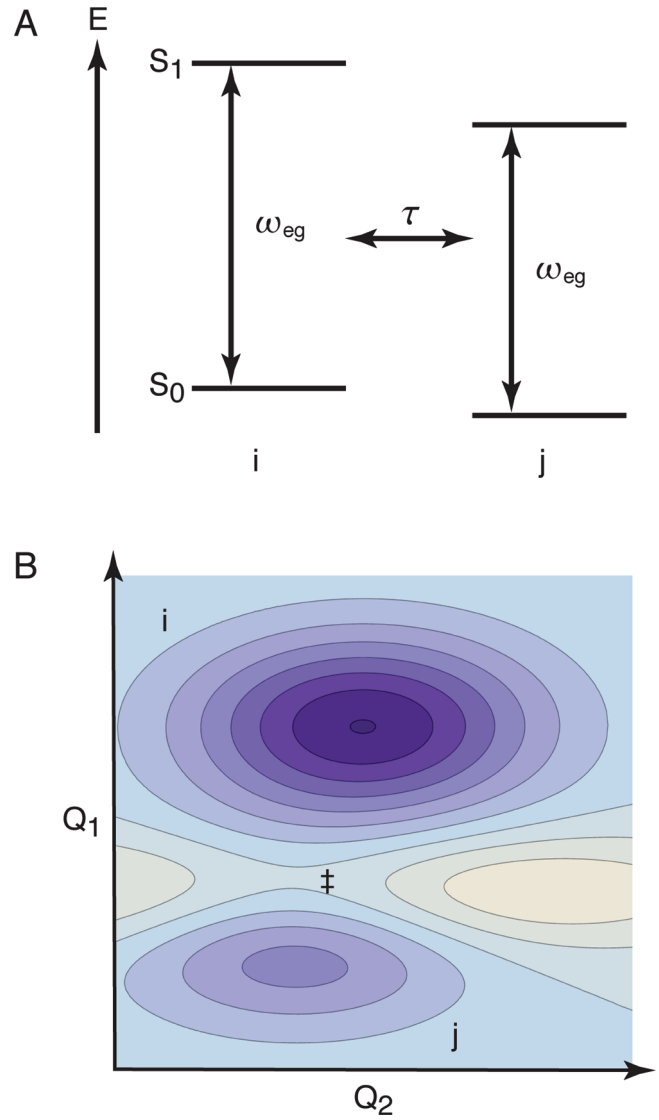

Figure 8. Model for equilibrium structural fluctuations in a protein involving barrier-crossing events: (a) Fluctuation with correlation time τ of the ground-to-excited-state energy gap ω_{eg} for an electronic probe coupled to motion of the protein between two structures at minima in the energy landscape, *i* and *j*; (b) Contour representation of the energy landscape with respect to two structural coordinates Q_1 and Q_2, showing minima for the structures *i* and *j* and a transition-state barrier, ‡, between them.

Figure 8 describes qualitatively how the ground-to-excited-state energy gap for an electronic probe responds to a fluctuation

of the structure of a protein. As the structure samples the energy landscape, it periodically passes over barriers in moving from one local free-energy minimum to the next. The presence of barriers can be inferred from the sensitivity of the correlation times to the external solvent friction or to internal (steric) friction[69,70] and/or from their temperature dependence.[71] If the displacement of the structure for a given motion results in a change of the local electric field at the position of the probe, the ground- and excited-state energy levels fluctuate synchronously; the energy gap between them is modulated because the dipole moment and polarizability of the probe are different in the two states.[72] The coupling strength $\langle(\Delta\omega)^2\rangle$ term in the energy-gap time-correlation function, $M(t)$ (eq 10), relates how strongly the energy gap fluctuates in response to the motion of the protein and its surrounding solvent. In analogy to the rotational motions sensed in FSS experiments on the ps time scale in polar liquids, the motions that would primarily be sensed in the FSS response in proteins in the >100-ps regime are librational (hindered rotational or torsional) in character.

In the theory discussed by García and Hummer[17] for a protein making diffusive motions with respect to its configurational coordinates, the resulting structural fluctuations are treated in terms of the stochastic displacements and velocities $x(t)$ and $\zeta(t)$ for a Brownian particle

$$x(t) = \int_0^t \zeta(t')\,dt' + x(0) \tag{12}$$

If $x(t)$ and $\zeta(t)$ are uncorrelated, the mean-square displacement for an ensemble of proteins is given by

$$\langle x^2(t)\rangle = \int_0^t dt' \int_0^{t'} dt'' \langle\zeta(t')\zeta(t'')\rangle \tag{13}$$

For Brownian motion, the derivative of the mean-square displacement with respect to time returns a diffusion constant D expressed in terms of $C(t)$, the time-correlation function for the velocity $\zeta(t)$

$$\frac{d}{dt}\langle x^2(t)\rangle = 2\int_0^t dt'\,\langle\zeta(t')\zeta(0)\rangle = 2\int_0^t dt'\,C(t') = 2D \tag{14}$$

This result has the important implication that Brownian motion is characterized by a linear relationship between the propagation time and the mean-square displacement[73]

$$\langle x^2(t)\rangle = 2Dt \tag{15}$$

The subdiffusion and superdiffusion regimes associated with motion impeded by traps or with longer range jumps over barriers, respectively, exhibit sublinear ($\langle x^2(t)\rangle \propto t^{n<1}$) or superlinear ($\langle x^2(t)\rangle \propto t^{n>1}$) dependences on time.[17]

The correlation time scale τ for a fluctuation can then be expressed by an Arrhenius expression

$$\tau = \tau_0 \exp(\Delta G^{\ddagger}/RT) \tag{16}$$

so that the correlation time increases as the barrier height $\Delta G^{\ddagger}$ increases. For Brownian diffusion, the transition-state structure at the peak of the barrier would be accessed at a characteristic time scale, τ_0, defined by the diffusion constant D and the mean-squared displacement, $\langle x^2(\tau_0)\rangle$

$$\tau_0 = \langle x^2(\tau_0)\rangle/2D \tag{17}$$

This result shows that the correlation time scale τ is linearly proportional to the mean-square displacement for the fluctuation. The diffusion constant D would be expected to be inversely proportional to the friction f[74]

$$D = k_B T/f \tag{18}$$

so an increase of friction would result in a lengthening of the correlation time. If the associated structural change for a fluctuation involves regions of the protein that are damped by the external solvent, as is observed for fbCytc and ZnCytc, τ_0 would be lengthened as the solvent friction increases.[6,69,70,75] If the solvent conditions are kept constant, however, a lengthening of the correlation time for a particular fluctuation would be consistent with an increase in the amplitude of the associated motion. Given that the barrier heights for motion on the energy landscape are likely to be strongly coupled to the conformational state, it should be clear that eq 17 provides only a rule-of-thumb for qualitative use in the interpretation of correlation time scales. Nevertheless, it is fully consistent with the observations made by Webb and co-workers using fluorescence correlation spectroscopy of fluctuations associated with conformational changes in apomyoglobin on the μs time scale.[76]

Comparison of the Solvation Response in fbCytc and ZnCytc. The FSS response from fbCytc and ZnCytc with the excitation laser tuned to the 0−0 vibronic transition in the Q band consists of monotonic biexponential shifts of the time-resolved fluorescence to lower energy. Because the observed shifts are relatively small, a few hundred cm^{-1} at most, the change in the porphyrin's dipole moment is relatively small, perhaps a few Debye, and because the porphyrin chromophore is relatively large, it is reasonable to assume that the linear-response regime is applicable. Note that in addition to the polar solvation response to the optical transition, there is also a nonnegligible nonpolar solvation response in ZnCytc that arises from the biphasic photodissociation of the axial ligands to the Zn^{II} ion, the histidine (H18) and methionine (M80) side chains. We consider this a nonpolar response because the size of the probe effectively increases as it throws off the axial ligands. The time scales associated with the response of the protein and the external solvent to the ligand photochemistry are apparently uncorrelated with the time scales for the FSS response.[16,23] As discussed in the Introduction, however, with excitation of ZnCytc into the Soret-band region of the absorption spectrum, the protein is launched along an unfolding trajectory along a pathway that successively populates at least three partially unfolded states. A similar unfolding process is apparently triggered in fbCytc at much lower excess vibrational excitations.[7,8] The assumption of linear response in the interpretation of the FSS response is obviously not valid if the laser excitation is tuned above the unfolding activation thresholds. In the present work, the excitation laser was tuned close to the 0−0 transition precisely to avoid this issue and to avoid adding a vibrational relaxation component to the observed FSS response. The time constants returned by the FSS response functions can then be considered the correlation times for two analogous classes of structural fluctuations in fbCytc and ZnCytc.

The model outlined above for the fluctuation time scales detected in the FSS response suggests a simple structural picture for the change in protein dynamics caused by demetalation of ZnCytc to form fbCytc. The observed correlation times are almost an order of magnitude longer in fbCytc than in ZnCytc, and there is no evidence that the components observed in ZnCytc are present but strongly attenuated in fbCytc. These results are consistent either with a significant increase in the structural amplitudes of the fluctuations of the hydrophobic core and solvent-contact regions or a significant increase in the height of the associated barriers. The former conclusion is obviously favored because the loss of the axial-ligand−metal interactions would, if anything, lower the barriers for motions of the folded protein orthogonal to the plane of the porphyrin (see Figure 1).

The MD simulations obtained for horse-heart FeCytc by García and Hummer[17] include fluctuations that are associated with transitions between local minima on the 100-ps time scale. The most active (largest mean-squared displacements) region of the structure in the MD trajectories is the region spanning amino-acid residues 36−61, which bridges the loops on the left and right-hand sides of the protein (as shown in Figure 1) that project the axial ligands (the side chains of H18 and M80, respectively) toward the metal ion. The latter region is associated with especially rapid hydrogen-exchange rates in the work by Englander and co-workers.[77]

The FSS responses observed in ZnCytc and fbCytc are well described by exponential components rather than by stretched exponentials or distributions of exponential components, which might be expected from a rough energy landscape characterized by a range of barrier heights.[78] Thus, the response in ZnCytc and fbCytc might be considered sparse; only two classes of motion are coupled significantly to the $\pi \rightarrow \pi^*$ transition of the intrinsic porphyrin in ZnCytc or fbCytc on the fluorescence time scale. It is likely that the motions that are detected in the FSS response are highly correlated motions: only the motions that result in coherent electric field fluctuations at the probe will have nonzero coupling strengths. Of course, groups in motion near to the probe would be expected to be more strongly coupled, but the low dielectric constant of the protein medium permits the motion of even distant charges or dipoles to be sensed. Noisy, uncorrelated motions will project incoherent electric field fluctuations that are canceled or attenuated when superimposed at the probe. The present results imply further that the fluorescence lifetime of the probe limits the detected response to a fairly narrow range of time scales. The mean-square displacements for the ps-ns motions we have detected in ZnCytc and fbCytc are probably fairly short-range in character, so they are likely to be associated with hindered torsional motions of the side chains of amino acids or of the polypeptide backbone. Future studies of the barrier heights associated with these correlation times through variation of the temperature, as in the work by Bhattacharyya and co-workers,[71] may provide some additional guidance for assignments of the character of motion.

Lastly, the conclusion that the fluctuations detected on the fluorescence time scale in fbCytc exhibit much larger mean-squared displacements than those in ZnCytc should be considered in the context of the dynamics for unfolding reactions. Barrier-crossing processes associated with diffusive motion along a generalized one-dimensional protein-folding reaction coordinate have been treated with transition-state theory expressions that are similar in form to that of eq 16.[6,79−81] The two correlation times observed in our fluorescence experiments probably arise from fluctuations along distinct structural coordinates near the native minimum of the energy landscape, and an association of either motion with the unfolding/refolding reaction coordinate requires additional information. As mentioned above, we observed previously that the enthalpies of activation for the partial unfolding transitions in fbCytc are about one-third of those measured in ZnCytc under the same solution conditions. The products of these unfolding reactions probably correspond to intermediates that are populated late along the folding pathway of FeCytc,[8] and the transition-state structures are likely to be found at small displacements from the native structure along coordinates that are perturbed by demetalation. It is accordingly reasonable to suggest that the short-range, metal-dependent fluctuations of the native structure observed in the FSS response function of fbCytc and ZnCytc are among those that promote the formation of the unfolding transition states under denaturing conditions and lead to longer-range unfolding/refolding motions on the μs-ms time scale.[82]

Acknowledgment. This research was supported by the National Science Foundation Biomolecular Systems Cluster/Molecular Biophysics program under grants MCB-050002 and MCB-0920101. We thank Professor Gary Blanchard (Michigan State University) for the use of the picosecond fluorescence spectrometer in his laboratory and for his technical assistance with the experiments.

References and Notes

(1) Bryngelson, J. D.; Wolynes, P. G. Spin glasses and the statistical mechanics of protein folding. *Proc. Natl. Acad. Sci. U.S.A.* **1987**, *84*, 7524–7528.

(2) Frauenfelder, H.; Sligar, S. G.; Wolynes, P. G. The energy landscapes and motions of proteins. *Science* **1991**, *254*, 1598–1603.

(3) Leopold, P. E.; Montal, M.; Onuchic, J. N. Protein folding funnels: a kinetic approach to the sequence-structure relationship. *Proc. Natl. Acad. Sci. U.S.A.* **1992**, *89*, 8721–8725.

(4) Ansari, A.; Berendzen, J.; Bowne, S. F.; Frauenfelder, H.; Iben, I. E.; Sauke, T. B.; Shyamsunder, E.; Young, R. D. Protein states and proteinquakes. *Proc. Natl. Acad. Sci. U.S.A.* **1985**, *82*, 5000–5004.

(5) Zwanzig, R. Diffusion in a rough potential. *Proc. Natl. Acad. Sci. U.S.A.* **1988**, *85*, 2029–2030.

(6) Socci, N. D.; Onuchic, J. N.; Wolynes, P. G. Diffusive dynamics of the reaction coordinate for protein folding funnels. *J. Chem. Phys.* **1996**, *104*, 5860–5868.

(7) Lampa-Pastirk, S.; Beck, W. F. Intramolecular vibrational preparation of the unfolding transition state of Zn^{II} substituted cytochrome *c*. *J. Phys. Chem. B* **2006**, *110*, 22971–22974.

(8) Barns, K. J.; Lampa-Pastirk, S.; Dillman, K. L.; Beck, W. F. Intramolecular vibrational excitation of unfolding reactions in Zn^{II}-substituted and metal-free cytochromes *c*: activation enthalpies from integrated fluorescence Stokes shift and lineshape excitation profiles. *J. Phys. Chem. B* **2008**, *112*, 15108–15115.

(9) Maroncelli, M. The dynamics of solvation in polar solvents. *J. Mol. Liq.* **1993**, *57*, 1–37.

(10) Stratt, R. M.; Maroncelli, M. Nonreactive dynamics in solution: the emerging molecular view of solvation dynamics and vibrational relaxation. *J. Phys. Chem.* **1996**, *100*, 12981–12996.

(11) Goto, Y.; Calciano, L. J.; Fink, A. L. Acid-induced folding of proteins. *Proc. Natl. Acad. Sci. U.S.A.* **1990**, *87*, 573–577.

(12) Tremain, S. M.; Kostić, N. M. Molten-globule and other conformational forms of zinc cytochrome *c*. Effect of partial and complete unfolding of the protein on its electron-transfer reactivity. *Inorg. Chem.* **2002**, *41*, 3291–3301.

(13) Lesch, H.; Stadlbauer, H.; Friedrich, J.; Vanderkooi, J. M. Stability diagram and unfolding of a modified cytochrome *c*: what happens in the transformation regime. *Biophys. J.* **2002**, *82*, 1644–1653.

(14) Fleming, G. R.; Cho, M. Chromophore-solvent dynamics. *Annu. Rev. Phys. Chem.* **1996**, *47*, 109–134.

(15) Bushnell, G. W.; Louie, G. V.; Brayer, G. D. High-resolution three-dimensional structure of horse heart cytochrome *c*. *J. Mol. Biol.* **1990**, *214*, 585–595.

(16) Lampa-Pastirk, S.; Beck, W. F. Polar solvation dynamics in Zn(II)-substituted cytochrome *c:* diffusive sampling of the energy landscape in the hydrophobic core and solvent-contact layer. *J. Phys. Chem. B* **2004**, *108*, 16288–16294.

(17) García, A. E.; Hummer, G. Conformational dynamics of cytochrome *c*: correlation to hydrogen exchange. *Proteins: Struct. Funct. Genet.* **1999**, *36*, 175–191.

(18) Vanderkooi, J. M.; Adar, F.; Ericińska, M. Metallocytochromes *c:* characterization of electronic absorption and emission spectra of Sn^{4+} and Zn^{2+} cytochromes *c*. *Eur. J. Biochem.* **1976**, *64*, 381–387.

(19) Vanderkooi, J. M.; Landesberg, R.; Hayden, G. W.; Owen, C. S. Metal-free and metal-substituted cytochromes *c.* Use in characterization of the cytochrome *c* binding site. *Eur. J. Biochem.* **1977**, *81*, 339–347.

(20) Elias, H.; Chou, M. H.; Winkler, J. R. Electron-transfer kinetics of Zn-substituted cytochrome *c* and its $Ru(NH_3)_5$ (Histidine-33) derivative. *J. Am. Chem. Soc.* **1988**, *110*, 429–434.

(21) Ye, S.; Shen, C.; Cotton, T. M.; Kostić, N. M. Characterization of zinc-substituted cytochrome *c* by circular dichroism and resonance Raman spectroscopic methods. *J. Inorg. Biochem.* **1997**, *65*, 219–226.

(22) Lakowicz, J. R. *Principles of Fluorescence Spectroscopy*, 2nd ed.; Kluwer Academic/Plenum Publishers: New York, 1999.

(23) Lampa-Pastirk, S.; Lafuente, R. C.; Beck, W. F. Excited-state axial-ligand photodissociation and nonpolar protein-matrix reorganization in Zn(II)-substituted cytochrome *c*. *J. Phys. Chem. B* **2004**, *108*, 12602–12607.

(24) Velapoldi, R. A.; Mielenz, K. D. *A Fluorescence Standard Reference Material: Quinine Sulfate Dihydrate*; National Bureau of Standards: Gaithersburg, MD, 1980.

(25) Cantor, C. R.; Schimmel, P. R. *Biophysical Chemistry. Part II: Techniques for the Study of Biological Structure and Function*; W. H. Freeman and Company: San Francisco, 1980.

(26) Siano, D. B.; Metzler, D. E. Band shapes of the electronic spectra of complex molecules. *J. Chem. Phys.* **1969**, *51*, 1856–1861.

(27) McHale, J. L. *Molecular Spectroscopy*; Prentice Hall: Upper Saddle River, NJ, 1999.

(28) Kennis, J. T. M.; Larsen, D. S.; Ohta, K.; Facciotti, M. T.; Glaeser, R. M.; Fleming, G. R. Ultrafast protein dynamics of bacteriorhodopsin probed by photon echo and transient absorption spectroscopy. *J. Phys. Chem. B.* **2002**, *106*, 6067–6080.

(29) Jordanides, X. J.; Lang, M. J.; Song, X.; Fleming, G. R. Solvation dynamics in protein environments studied by photon echo spectroscopy. *J. Phys. Chem. B* **1999**, *103*, 7995–8005.

(30) Simon, J. D.; Thompson, P. A. Spectroscopy and rotational diffusion of oxazine 725 in alcohols: a test of dielectric friction theories. *J. Chem. Phys.* **1990**, *92*, 2891–2896.

(31) Maroncelli, M.; Fleming, G. R. Picosecond solvation dynamics of coumarin 153: the importance of molecular aspects of solvation. *J. Chem. Phys.* **1987**, *86*, 6221–6239.

(32) Åkerlöf, G. Dielectric constants of some organic solvent-water mixtures at various tempeatures. *J. Am. Chem. Soc.* **1932**, *54*, 4125–4139.

(33) Scholte, T. G. Relation between the refractive index increment and the density increment of binary mixtures: application to the determination of partial specific volumes of polymers in solution. *J. Polymer Sci. A-2* **1972**, *10*, 519–526.

(34) Toptygin, D.; Woolf, T. B.; Brand, L. Picosecond protein dynamics: the origin of the time-dependent spectral shift in the fluorescence of the single Trp in the protein GB1. *J. Phys. Chem. B* **2010**, *114*, 11323–11337.

(35) Toptygin, D.; Savtchenko, R. S.; Meadow, N. D.; Brand, L. Homogeneous spectrally- and time-resolved fluorescence emission from single-tryptophan mutants of IIA^{Glc} protein. *J. Phys. Chem. B* **2001**, *105*, 2043–2055.

(36) Vincent, M.; Gilles, A.-M.; de la Sierra, I. M. L.; Briozzo, P.; Bârzu, O.; Gallay, J. Nanosecond fluorescence dynamic Stokes shift of tryptophan in a protein matrix. *J. Phys. Chem. B* **2000**, *104*, 11286–11295.

(37) Cho, B. M.; Carlsson, F.; Jimenez, R. Photon echo spectroscopy of porphyrins and heme proteins: effects of quasidegenerate electronic structure on the peak shift decay. *J. Chem. Phys.* **2006**, *124*, 144905.

(38) Maroncelli, M.; MacInnis, J.; Fleming, G. R. Polar solvent dynamics and electron-transfer reactions. *Science* **1989**, *243*, 1674–1681.

(39) Carter, E. A.; Hynes, J. T. Solvation dynamics for an ion pair in a polar solvent: time-dependent fluorescence and photochemical charge transfer. *J. Chem. Phys.* **1991**, *94*, 5961–5979.

(40) Rosenthal, S. J.; Xie, X.; Du, M.; Fleming, G. R. Femtosecond solvation dynamics in acetonitrile: observation of the inertial contribution to the solvent response. *J. Chem. Phys.* **1991**, *95*, 4715–4718.

(41) Jimenez, R.; Fleming, G. R.; Kumar, P. V.; Maroncelli, M. Femtosecond solvation dynamics of water. *Nature* **1994**, *369*, 471–473.

(42) Stratt, R. M.; Cho, M. The short-time dynamics of solvation. *J. Chem. Phys.* **1994**, *100*, 6700–6708.

(43) Maroncelli, M.; Kumar, P. V.; Papazyan, A.; Horng, M. L.; Rosenthal, S. J.; Fleming, G. R. Studies of the inertial component of polar solvation dynamics. In *Ultrafast Reaction Dynamics and Solvent Effects*; Guaduel, Y., Rossky, P. J., Eds.; AIP Press: Woodbury, NY, 1994; pp 310−333.

(44) Ladanyi, B. M.; Stratt, R. M. Short-time dynamics of solvation: linear solvation theory for polar solvents. *J. Phys. Chem.* **1995**, *99*, 2502–2511.

(45) Joo, T.; Jia, Y.; Yu, J.-Y.; Lang, M. J.; Fleming, G. R. Third-order nonlinear time domain probes of solvation dynamics. *J. Chem. Phys.* **1996**, *104*, 6089–6108.

(46) Cho, M.; Yu, J.-Y.; Joo, T.; Nagasawa, Y.; Passino, S. A.; Fleming, G. R. The integrated photon echo and solvation dynamics. *J. Phys. Chem.* **1996**, *100*, 11944–11953.

(47) Barthel, E. R.; Martini, I. B.; Schwartz, B. J. How does the solvent control electron transfer? Experimental and theoretical studies of the simplest charge transfer reaction. *J. Phys. Chem. B* **2001**, *105*, 12230–12241.

(48) Nilsson, L.; Halle, B. Molecular origin of time-dependent fluorescence shifts in proteins. *Proc. Natl. Acad. Sci. U.S.A.* **2005**, *102*, 13867–13872.

(49) Homoelle, B. J.; Edington, M. D.; Diffey, W. M.; Beck, W. F. Stimulated photon-echo and transient-grating studies of protein-matrix solvation dynamics and interexciton-state radiationless decay in α phycocyanin and allophycocyanin. *J. Phys. Chem. B* **1998**, *102*, 3044–3052.

(50) Jimenez, R.; Romesberg, F. E. Excited state dynamics and heterogeneity of folded and unfolded states of cytochrome *c*. *J. Phys. Chem. B* **2002**, *106*, 9172–9180.

(51) Riter, R. E.; Edington, M. D.; Beck, W. F. Inertial protein-matrix solvation of a light-harvesting chromophore. In *Ultrafast Phenomena X*; Barbara, P., Knox, W., Zinth, W., Fujimoto, J., Eds.; Springer-Verlag: Berlin, 1996; pp 324−325.

(52) Riter, R. E.; Edington, M. D.; Beck, W. F. Protein-matrix solvation dynamics in the α subunit of *C*-phycocyanin. *J. Phys. Chem.* **1996**, *100*, 14198–14205.

(53) Pal, S. K.; Peon, J.; Bagchi, B.; Zewail, A. H. Biological water: femtosecond dynamics of macromolecular hydration. *J. Phys. Chem. B* **2002**, *106*, 12376–12395.

(54) Pal, S. K.; Peon, J.; Zewail, A. H. Biological water at the protein surface: dynamical solvation probed directly with femtosecond resolution. *Proc. Natl. Acad. Sci. U.S.A.* **2002**, *99*, 1763–1768.

(55) Qiu, W.; Zhang, L.; Okobia, O.; Yang, Y.; Wang, L.; Zhong, D.; Zewail, A. H. Ultrafast solvation dynamics of human serum albumin: correlations with conformational transitions and site-selected recognition. *J. Phys. Chem. B* **2006**, *110*, 10540–10549.

(56) Abbyad, P.; Shi, X.; Childs, W.; McAnaney, T. B.; Cohen, B. E.; Boxer, S. G. Measurement of solvation responses at multiple sites in a globular protein. *J. Phys. Chem. B* **2007**, *111*, 8269–8276.

(57) Abbyad, P.; Childs, W.; Shi, X.; Boxer, S. G. Dynamic Stokes shift in green fluorescent protein variants. *Proc. Natl. Acad. Sci. U.S.A.* **2007**, *104*, 20189–20194.

(58) Halder, M.; Mukherjee, P.; Bose, S.; Hargrove, M. S.; Song, X.; Petrich, J. W. Solvation dynamics in protein environments: comparison of fluorescence upconversion measurements of coumarin 153 in monomeric hemeproteins with molecular dynamics simulations. *J. Chem. Phys.* **2007**, *127*, 055101−1-6.

(59) Lang, M. J.; Jordanides, X. J.; Song, X.; Fleming, G. R. Aqueous solvation dynamics studied by photon echo spectroscopy. *J. Chem. Phys.* **1999**, *110*, 5884–5892.

(60) Simonson, T. Gaussian fluctuations and linear response in an electron transfer protein. *Proc. Natl. Acad. Sci. U.S.A.* **2002**, *99*, 6544–6549.

(61) Bagchi, B. Water solvation dynamics in the bulk and in the hydration layer of proteins and self-assemblies. *Annu. Rep. Prog. Chem. Sect. C* **2003**, *99*, 127–175.

(62) Bagchi, B. Water dynamics in the hydration layer around proteins and micelles. *Chem. Rev.* **2003**, *105*, 3197–3219.

(63) Li, T.; Kao, Y.-T.; Zhong, D.; Singer, S. J. Hydration dynamics and time scales of coupled water-protein fluctuations. *J. Am. Chem. Soc.* **2007**, *129*, 3376–3382.

(64) Bashkin, J. S.; McLendon, G.; Mukamel, S.; Marohn, J. Influence of medium dynamics on solvation and charge separation reactions: comparison of a simple alcohol and a protein "solvent". *J. Phys. Chem.* **1990**, *94*, 4757–4761.

(65) Pierce, D. W.; Boxer, S. G. Dielectric relaxation in a protein matrix. *J. Phys. Chem.* **1992**, *96*, 5560–5566.

(66) Toptygin, D.; Gronenborn, A. M.; Brand, L. Nanosecond relaxation dynamics of protein GB1 identified by the time-dependent red shift in the fluorescence of tryptophan and 5-fluorotryptophan. *J. Phys. Chem. B.* **2006**, *110*, 26292–26302.

(67) Cohen, B. E.; McAnaney, T. B.; Park, E. S.; Jan, Y. N.; Boxer, S. G.; Jan, L. Y. Probing protein electrostatics with a synthetic fluorescent amino acid. *Science* **2002**, *296*, 1700–1703.

(68) Golosov, A. A.; Karplus, M. Probing polar solvation dynamics in proteins: A molecular dynamics simulation analysis. *J. Phys. Chem. B* **2007**, *111*, 1482–1490.

(69) Beece, D.; Eisenstein, L.; Frauenfelder, H.; Good, D.; Marden, M. C.; Reinisch, L.; Reynolds, A. H.; Sorensen, L. B.; Yue, K. T. Solvent viscosity and protein dynamics. *Biochemistry* **1980**, *19*, 5147–5157.

(70) Ansari, A.; Jones, C. M.; Henry, E. R.; Hofrichter, J.; Eaton, W. A. The role of solvent viscosity in the dynamics of protein conformational changes. *Science* **1992**, *256*, 1796–1798.

(71) Sahu, K.; Mondal, S. K.; Ghosh, S.; Roy, D.; Bhattacharyya, K. Temperature dependence of solvation dynamics and anisotropy decay in a protein: ANS in bovine serum albumin. *J. Chem. Phys.* **2006**, *124*, 124909.

(72) Kumar, P. V.; Maroncelli, M. Polar solvation dynamics of polyatomic solutes: simulation studies in acetonitrile and methanol. *J. Chem. Phys.* **1995**, *103*, 3038–3060.

(73) Berry, R. S.; Rice, S. A.; Ross, J. *Physical Chemistry*; John Wiley & Sons: New York, 1980.

(74) McQuarrie, D. A. *Statistical Mechanics*; HarperCollins Publishers: New York, 1976.

(75) Frauenfelder, H.; Chen, G.; Berendzen, J.; Fenimore, P. W.; Jansson, H.; McMahon, B. H.; Stroe, I. R.; Swenson, J.; Young, R. D. A unified model of protein dynamics. *Proc. Natl. Acad. Sci. U.S.A.* **2009**, *106*, 5129–5134.

(76) Chen, H.; Rhoades, E.; Butler, J. S.; Loh, S. N.; Webb, W. W. Dynamics of equilibrium structural fluctuations of apomyoglobin measured by fluorescence correlation spectroscopy. *Proc. Natl. Acad. Sci. U.S.A.* **2007**, *104*, 10459–10464.

(77) Bai, Y.; Sosnice, T. R.; Mayne, L.; Englander, S. W. Protein folding intermediates: native-state hydrogen exchange. *Science* **1995**, *269*, 192–197.

(78) Carlini, P.; Bizzarri, A. R.; Cannistraro, S. Temporal fluctuations in the potential energy of proteins: $1/f^{\alpha}$ noise and diffusion. *Physica D* **2002**, *165*, 242–250.

(79) Nettels, D.; Gopich, I. V.; Hoffmann, A.; Schuler, B. Ultrafast dynamics of protein collapse from single-molecule photon statistics. *Proc. Natl. Acad. Sci. U.S.A.* **2007**, *104*, 2655–2660.

(80) Cellmer, T.; Henry, E. R.; Hofrichter, J.; Eaton, W. A. Measuring internal friction of an ultrafast-folding protein. *Proc. Natl. Acad. Sci. U.S.A.* **2008**, *105*, 18320–18325.

(81) Best, R. B.; Hummer, G. Coordinate-dependent diffusion in protein folding. *Proc. Natl. Acad. Sci. U.S.A.* **2010**, *107*, 1088–1093.

(82) Henzler-Wildman, K. A.; Lei, M.; Thai, V.; Kerns, S. J.; Karplus, M.; Kern, D. A hierarchy of timescales in protein dynamics is linked to enzyme catalysis. *Nature* **2007**, *450*, 913–916.

JP1044964